24th INTERNATIONAL CONGRESS ON SOUND AND VIBRATION
23–27 July 2017, London

ICSV24
23-27JULY 2017
LONDON CALLING

VALIDATION OF A WAVELET DECONVOLUTION METHOD FOR EXPERIMENTAL DETERMINATION OF THE FORCE APPLIED BY LIQUID WATER DROPS

Yicheng Yu, Carl Hopkins

Acoustics Research Unit, School of Architecture, University of Liverpool, Liverpool L69 7ZN, UK
email: yuy@liverpool.ac.uk, carl.hopkins@liverpool.ac.uk

The time-dependent force applied by liquid drops of water impacting on a structure is required to predict the resulting vibration and radiated sound. Previous work has used idealizations of the drop shape in order to predict this force. To assess the validity of such idealized models, the time-varying force applied by a single water drop falling onto a dry sheet of 6mm glass has been determined experimentally using a wavelet deconvolution method. To validate this approach the force is also measured using a glass-steel disc attached to a force transducer. In these experiments, 2mm and 4.5mm diameter drops were released from various heights to achieve drop velocities up to values which are close to terminal velocity. Differences between the wavelet estimation and force transducer results were less than 2.5 dB in the energy spectral density over the frequency range from 10 to 6k Hz. The validated wavelet dataset has been used to determine empirical equations for the time-dependent force applied by a water drop on a dry surface.

Keywords: rain, water drop, wavelet, impact force

1. Introduction

This paper concerns measurement of the time-dependent force applied by a falling drop of water on a sheet of glass that could subsequently be used to predict the resulting sound and vibration.

Previous measurements have used a variety of approaches to quantify the time-dependent force from a liquid drop. Nearing *et al* [1] used pressure sensors to measure water-drop impact forces from which they noted that the time-dependent force and average pressure was not adequately predicted by theory based on incompressible mechanics or numerical techniques which do not account for compressional wave generation, surface tension, and viscosity. Nearing and Bradford [2] used empirical equations to predict the peak force for which the regression curves had high correlation coefficients. Grinspan and Gnanamoorthy [3] used PVDF film to measure the impact force applied by a low velocity water drop and oil droplet on a solid surface. This showed that the impact force depends on the impact velocity and density of the liquid. Soto *et al* [4] used two different approaches to measure the impact force from a rain drop: a piezoelectric quartz and a thin glass lamella. The latter approach used mechanical equilibrium to determine the maximum force from the largest deformation of the lamella for a given impact. Most approaches have used a piezoelectric transducer to obtain the time-dependent force which is sometimes problematic if affected by resonances of the transducer disc (e.g. [5]). To avoid such issues, Doyle's wavelet deconvolution method [6] is applied as an inverse method in this paper to estimate the time-dependent force. This approach is advantageous because of its robustness to noise, and the ability to use a rigid glass surface which provides the appropriate driving-point mobility and surface condition of interest in terms of roughness, wettability and surface water.

Based on experimental observations, idealized drop shape models have been used to predict the time-dependent force. Petersson [7] compared paraboloidal and cylindrical-hemispherical drop shapes with measurements for which the former shape showed better agreement than the latter. This was in conflict with photographic observations in the literature (e.g. [5]) from which the cylindrical-hemispherical model would have been expected to be more appropriate. The problem with this model was attributed to the assumption of constant velocity in the flow phase. Petersson also showed that both the receiver impedance and a flow impedance must be considered when calculating the injected power into a structure unless one is significantly smaller than the other. Roisman *et al* [8] assumed a spherical drop shape model to estimate the normal impact spreading and receding phenomenon from which the time-dependent force was derived, but not compared with measurements. Anantharamaiah *et al* [9] later compared the calculated force from Roisman *et al* with their CFD simulations, which showed close agreement for a 4.9mm diameter water drop at a drop velocity of 2.34m/s (i.e. well-below terminal velocity).

Suga and Tachibana [10] used the paraboloidal model from Petersson to estimate the injected power from natural rainfall but only made one indirect comparison of theory with laboratory measurements. Hopkins [11] also used the paraboloidal drop shape model and Statistical Energy Analysis (SEA) to predict the radiated sound of a glass plate which showed close agreement with measurements below 800Hz and above 1.6kHz. However, in the intermediate frequency range, there was a discrepancy that could possibly be caused by the choice of idealized drop shape or the lack of consideration of surface water on the glass. The paraboloidal and cylindrical-hemisphere drop shape models are not particularly realistic because most drops are approximately spherical before impact, although drops can be rendered ellipsoidal by aerodynamic forces [12]. In this paper the issues with seeking idealized drop shape models for different drop velocities are avoided by determining an empirical model for the time-dependent force.

In the first part of this paper, the time-dependent force applied by a drop of water falling onto a sheet of glass is measured using wavelet deconvolution and validated against measurements using a glass disc fixed to a force transducer. The time-dependent force is then compared with predictions assuming idealized drop shapes from the literature. The validated wavelet results are used to produce an improved empirical model for the time-dependent force.

2. Wavelet deconvolution

When an unknown impact force excites an LTI system, a matrix of transfer accelerances, $\mathbf{H}$, describes the response, $\mathbf{e}$, at points on this system to this impact force $\mathbf{f}$, by a linear convolution integral for which the discrete time domain response can be expressed as:

$$\mathbf{e} = \mathbf{H}\mathbf{f} + \mathbf{n} \tag{1}$$

Without noise, the original force can be estimated by [6]:

$$\mathbf{f} = \mathbf{\Phi}^{\mathbf{H}}\mathbf{f}_{\mathbf{w}} = \mathbf{\Phi}^{\mathbf{H}}(\mathbf{\Psi}\mathbf{\Psi}^{\mathbf{H}})^{-\mathbf{1}}\mathbf{\Psi}\mathbf{e} \tag{2}$$

where $\mathbf{f}_{\mathbf{w}}$ is a vector with dimension M to replace the original unknown vector $\mathbf{f}$ with dimension N, $\mathbf{\Phi}_{M\times N}$ is a matrix of wavelet functions: $\phi_m(t_n) = \exp[-\left(\frac{t_n - mt_0}{\alpha}\right)^2]$, $\mathbf{\Psi}_{M\times N} = \mathbf{\Phi}\mathbf{H}^{\mathbf{H}}$ is a matrix of functions $\psi_m(t_n) = \sum_{k=1}^{n} h(t_n - \tau_k)\phi_m(\tau_k)$.

With noise, $\mathbf{n}$, Eq. (1) can be rewritten as:

$$\mathbf{e} = \mathbf{H}\mathbf{\Phi}^{\mathbf{H}}\mathbf{f}_{\mathbf{w}} + \mathbf{n} = \mathbf{\Psi}^{\mathbf{H}}\mathbf{f}_{\mathbf{w}} + \mathbf{n} \tag{3}$$

Now consider the estimation of M-dimensional random parameter vector $\mathbf{f}_{\mathbf{w}}$ from an N-dimensional observation vector $\mathbf{e}$. Assuming that the matrix $\mathbf{\Psi}^{\mathbf{H}} = \mathbf{H}\mathbf{\Phi}^{\mathbf{H}}$ is known, and that the noise is a Gaussian-distributed, random process with mean $\boldsymbol{\mu}_{\mathbf{n}}$, and covariance matrix $\mathbf{\Sigma}_{\mathbf{nn}}$, the Maximum Likelihood Estimate (MLE) obtained from maximization of the log-likelihood function $\ln[f_{\mathbf{E}|\mathbf{F}_{\mathbf{w}}}(\mathbf{e}|\mathbf{f}_{\mathbf{w}})]$ with respect to $\mathbf{f}_{\mathbf{w}}$ is given by [13]:

$$\mathbf{\Psi}\mathbf{\Psi}^{\mathbf{H}}\mathbf{f}_{\mathbf{w}} = \mathbf{\Psi}(\mathbf{e} - \boldsymbol{\mu}_{\mathbf{n}}) \tag{4}$$

$$\xrightarrow{well-posed\ \mathbf{\Psi}\mathbf{\Psi}^{\mathbf{H}}} \mathbf{f}_{\mathbf{w}} = (\mathbf{\Psi}\mathbf{\Psi}^{\mathbf{H}})^{-1}\mathbf{\Psi}(\mathbf{e} - \boldsymbol{\mu}_{\mathbf{n}}) \tag{5}$$

If $\boldsymbol{\mu}_{\mathbf{n}} = 0$, then the noise is white Gaussian with a mean value of zero and Eq. (5) should be the same as Eq. (2). In practice matrix $\boldsymbol{\Psi}\boldsymbol{\Psi}^{\mathbf{H}}$ can be ill-conditioned (for example, in our experiment, the plate is highly damped which makes **H** sparse). Considering the equivalence between MLE and Least Square Estimation (LSE) in the presence of Gaussian noise, the LSQR algorithm [14] is used to solve Eq. (4) to give $\mathbf{f}_{\mathbf{w}}$.

The system impulse response can be measured using force hammer excitation with accelerometers at a number of response points. The unknown force applied by the real impact can then be related to the impact force, $\bar{\mathbf{f}}$, applied by the force hammer, and $\bar{\mathbf{e}}$ the associated acceleration signal [15] by

$$\mathbf{e} * \bar{\mathbf{f}} = \bar{\mathbf{e}} * \mathbf{f} \tag{6}$$

Substituting Eq. (6) into Eq. (4) or (5) means that matrix **H** can be obtained from the vector $\bar{\mathbf{e}}$**.**

3. Experimental set-up

The experimental work uses 4.5mm and 2mm diameter drops of reverse osmosis water. The 4.5mm drops are produced from a 50mL burette with a needle attachment to produce the 2mm drops. To ensure repeatable drops, a relatively slow drop formation time was used, ranging from 10s to 1min [16]. To achieve a range of drop velocities up to terminal velocity, drop heights were chosen up to 6.5m. During the fall, each drop travels within plastic tubing (7m length, 200mm diameter) to minimise any influence from air movement in the laboratory. This ensures that the drop velocity and excitation position are repeatable. The drop diameters are measured using two different approaches: (1) by calibrating the frame dimension of a high-speed camera (Lambda Mega Speed HHC X2) to capture an image of the drop just before impact, and (2) measuring the total mass of 200 drops and calculating the diameter. There is less than 0.05mm difference between the drop diameter determined using these two methods. The velocity of the impact drops is also measured using the high-speed camera, with the maximum error being less than 8.3%. All experiments were carried out at temperatures between 21^{o}C and 25^{o}C, and relative humidity between 40% and 60%. Before each measurement, all glassware is cleaned and dried.

All signals are recorded using a B&K Pulse Analyser with a sample rate of 1.31E5 Hz, a low-frequency cut-off of 10 Hz, and a high-frequency cut-off of 10k Hz.

Wavelet deconvolution measurements use a 6mm thick glass plate (1.2m×1m) with the response measured using accelerometers (B&K 4375) superglued to the underside of the glass plate at three randomly located positions. Damping around the plate boundaries is achieved using a continuous 50mm wide strip clamped by 13mm thick strips of Sylomer SR55 compressed with 13mm thick steel. The transfer matrix **H** from impact force at the excitation position p_e to acceleration at sensing positions p_{1-3} was measured using a force hammer (B&K Type 8203). Using Eqs. (5-6), three force pulse curves are calculated and averaged using the transfer matrix and the response signal is measured at three different sensing positions. Time domain averaging is used with impacts from eight drops.

The force transducer disc measurement uses a 6mm thick glass disc superglued to a 6mm steel disc to ensure that the surface condition is identical in terms of wettability and roughness to the wavelet deconvolution measurements. The 30mm disc diameter is sufficient to keep the spreading liquid within the disc. The disc is screwed to a force transducer (B&K Type 8200) which was mounted on a heavy mass-spring system to reduce the level of background vibration. However, the first structural mode of the transducer-disc system causes ringing between 7.5k and 8.5k Hz. Hence a second-order, band-stop Butterworth filter (low-frequency cut-off at 7k Hz, high-frequency cut-off at 9k Hz) is used to remove the ringing without significantly changing the force below 6k Hz.

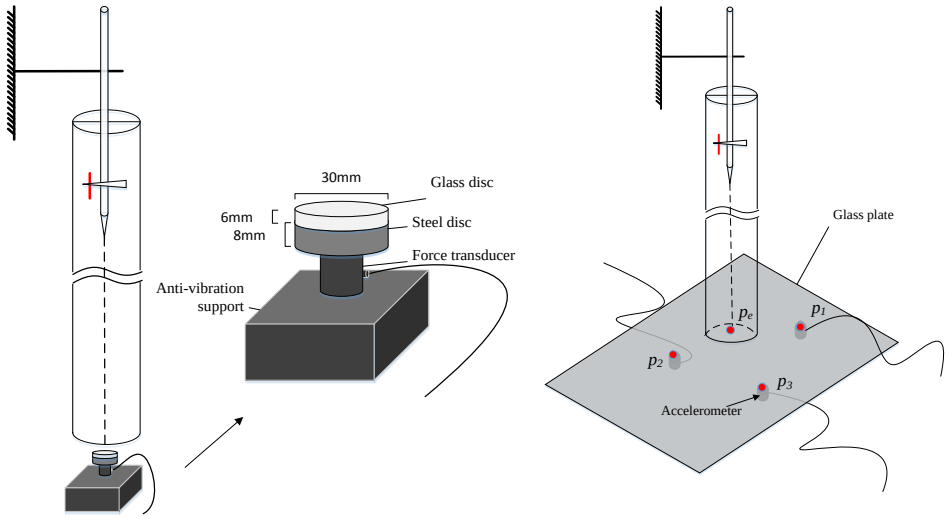

(a) (b)

Figure 1. Measurement set-ups: (a) force transducer disc, (b) glass plate used for wavelet deconvolution.

4. Empirical formulae based on wavelet measurements

The wavelet measurements are used to determine an empirical formula using the following three steps:

1) Assume that the formula is dependent on three parameters:
$$F(t) = F(t; C, \mu, \sigma) = C \exp[(-\ln(1000t) + \mu)/\sigma^2]^2$$
2) Minimise the absolute error (2-norm) between this formula and the measured wavelet data gives the optimized parameters: C, μ, σ
$$\arg\min_{C,\mu,\sigma} \|f(t; C, \mu, \sigma) - f_{\text{wavelet}}(t)\|_2$$
3) Use a polynomial fitting function to give the relationship between the parameters $\ln(C), \mu, \sigma$ and the drop velocity v with the least squares approach as
$$\ln(C) = a_C * v + b_C$$
$$\mu = a_\mu * v + b_\mu$$
$$\sigma = a_\mu * v + b_\mu$$

5. Results and discussion

5.1 Drop shape

Theoretical and numerical research tends to be based on the assumption that drops are spherical, when moving in a homogeneous, unlimited ambient medium, and interfacial tension and/or viscous forces are much more important than inertia forces [12,17,18]. For high Reynolds number (Re>10^3), the initial spherical drop shape becomes distorted [17]. For heavy rain, the diameter of raindrops is assumed to be 5mm [11], which is close to the artificial drop of 4.5mm used in this paper. These 4.5mm drops travelled at 8.2m/s which is slightly slower than their terminal velocity of 9.0m/s. However, assuming that their shape would be similar to those at terminal velocity, their shape was estimated by combining two halves of different oblate spheroids according to [17]. Figure 2 shows a photograph of the 4.5mm drop captured by high-speed camera and the estimated shape; they are slightly different which is attributed to the different velocities. The axis ratio is defined as the ratio of the largest vertical and horizontal chords of the drop commonly used to describe the equilibrium drop shape [18,19]. According to [19], the axis ratio of 2mm drops at terminal velocity is about 0.91, which is approximately spherical. Therefore, in these experiments only the axis ratios for 4.5mm drops are shown in Table 1. For drop heights of 0.41, 0.81 and 1.63m (corresponding to drop velocities of 2.69, 3.77, 5.18m/s) the drops are approximately spherical (within experimental

error and variation due to drop oscillations), but the shape becomes increasingly flattened at heights of 3.25 and 6.5m (corresponding to 6.73 and 8.20m/s).

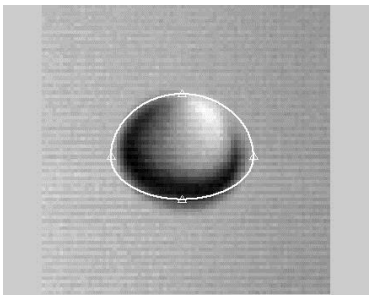

Figure 2. Estimated drop shape for a 4.5mm water drop from [15] at terminal velocity of 9.0m/s (white line), and an actual drop captured by high speed camera in the experiments with a velocity of 8.2m/s.

Table 1. Axis ratio of 4.5mm drops (average of seven measurements) at different drop heights, *H*.

	H = 0.41m	*H* = 0.81m	*H* = 1.63m	*H* = 3.25m	*H* = 6.5m
Mean axis ratio	0.98	0.96	0.95	0.86	0.79
Standard deviation	0.072	0.034	0.039	0.045	0.064
Maximum axis ratio	1.08	1	1.06	0.93	0.93
Minimum axis ratio	0.93	0.93	0.93	0.81	0.73

5.2 Comparison of measured forces near terminal velocity

Water drop velocities are shown in Table 2. These were measured just before impact using a high-speed camera from which average values were determined from ten drops at each drop height. Heights were chosen to give a range of velocities up to near terminal velocity (6.4m/s for 2mm drops, 9.0m/s for 4.5mm). For 2mm and 4.5mm drops travelling at approximately terminal velocity, Fig. 3 shows high-speed camera shots indicating that 0.2ms before impact the water drop shape has become slightly distorted from the idealized spherical shape.

Table 2. Measured water drop velocities (m/s) before impact for the different drop heights, *H*.

	H = 0.41m	*H* = 0.81m	*H* = 1.63m	*H* = 3.25m	*H* = 6.5m
2mm drop	2.06	3.49	4.62	5.71	-----
4.5mm drop	2.69	3.77	5.18	6.73	8.20

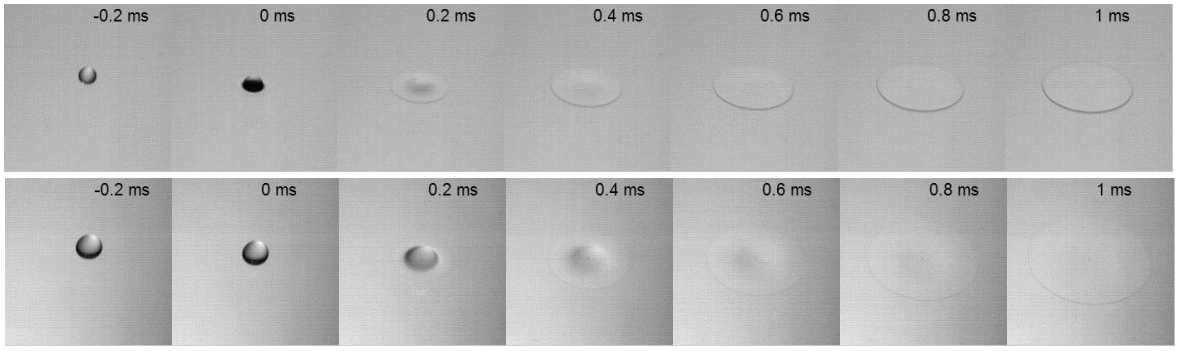

Figure 3. Photographs of the drop before, at and after impact on the dry glass plate where impact occurs at 0ms: (a) 2mm drop released from a height of 3.25m, (b) 4.5mm drop released from a height of 6.5m.

Figures 4(a) and 5(a) show the measured time-dependent forces from the 2mm and 4.5mm diameter drops respectively. Close agreement is observed between the wavelet and force transducer measurements although there was a difference in the initial slope in Fig. 5(a) due to the band-stop filter used with the force transducer. When the water drop hits the glass surface, the force pulse in-

creases rapidly during the first 0.1ms which could be due to “water hammer” [3] or compressibility of the water drop [1]. Approximately 0.1ms after the initial contact, the force deceases as the liquid begins to spread outward.

Comparison of measurements with the idealised models for the paraboloidal, cylindrical-hemispherical, and spherical shapes, or using a combined ellipsoidal drop shape [17] indicate that the idealised drop shapes do not take account of the compressibility of the liquid and assume that the spreading liquid in the drop “disappears” [5], which may cause a lower estimation of the force peak. The model from Roisman *et al* [7] takes the spreading lamella into account which is beneficial as it leads to a slightly higher peak force than the other idealized shape models; however, the peak force for the 4.5mm drop at 8.2m/s is still significantly underestimated – see Fig. 5(a).

The Energy Spectral Density (ESD) is shown in Figs. 4(b) and 5(b) for 2mm and 4.5mm drop diameter respectively. The time-dependent force is zero-padded after the first zero crossing to avoid ringing and background noise from the force transducer, and to increase the frequency resolution. Differences between wavelet and force transducer measurements are typically <2.5dB. It is seen that the five idealised drop shape models are unable to reproduce the measured spectrum.

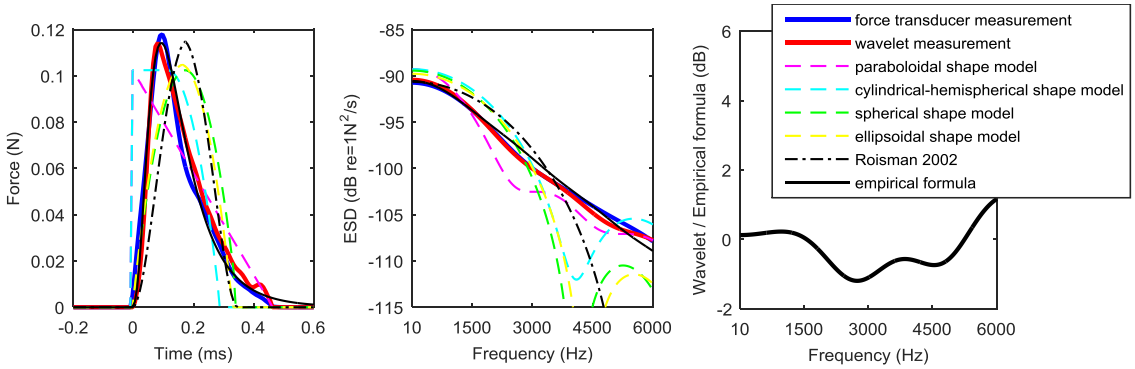

(a) (b) (c)

Figure 4. 2mm drops released from 3.25m height with impact on dry glass surface：(a) time-dependent force (b) energy spectrum density (10 - 6k Hz), (c) the difference between wavelet and empirical formula ESD. Solid line: Force transducer measured data (blue solid line); wavelet measured data (red solid line). Dashed line: paraboloidal shape model (magenta dashed line); cylindrical-hemispherical shape model (cyan dashed line); spherical shape model (green dashed line); ellipsoidal shape model (yellow dashed line). Dot-dashed line: Equations from [7, 8]. Black solid line: empirical formula estimated: black line.

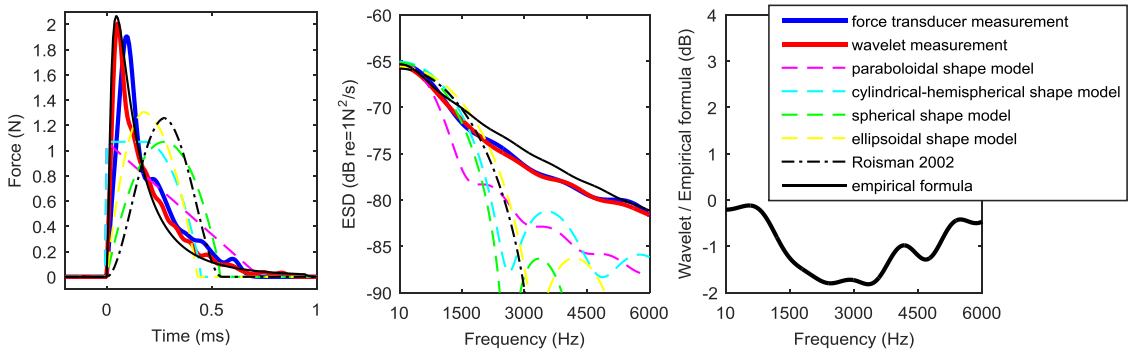

(a) (b) (c)

Figure 5. 4.5mm drops released from 6.5m height with impact on dry glass surface：(a) time-dependent force (b) energy spectrum density (10 - 6k Hz), (c) the difference between wavelet and empirical formula ESD. Solid line: Force transducer measured data (blue solid line); wavelet measured data (red solid line). Dashed line: paraboloidal shape model (magenta dashed line); cylindrical-hemispherical shape model (cyan dashed line); spherical shape model (green dashed line); ellipsoidal shape model (yellow dashed line). Dot-dashed line: Equations from [7, 8]. Black solid line: empirical formula estimated: black line.

The empirical formula for the time-dependent force is:

$$F(t) = C \exp[(-\ln(1000t) + \mu)/\sigma^2]^2$$

where

$C = \exp(0.451 * v - 4.745)$, $\mu = 2.2$, $\sigma = -0.181 * v + 1.832$ for 2mm drops, and

$C = \exp(0.485 * v - 3.25)$, $\mu = (v + 1.01)/3$, $\sigma = 1.4$ for 4.5mm drops.

Figs 4(c) and 5(c) show that the empirical formula reproduces the wavelet measurements within 2dB for 2mm and 4.5mm diameter drops respectively.

5.3 Comparison of measured impact forces at different drop velocities

Figures 6 and 7 show that the peak in the time-dependent force increases with increasing drop velocity. The differences between wavelet and force transducer measurements are <2.5 dB except at the lowest drop velocity for which the wavelet measurement is slightly lower than the force transducer measurement at high frequencies. This is due to the modal response of the disc (despite the use of the band-stop filter).

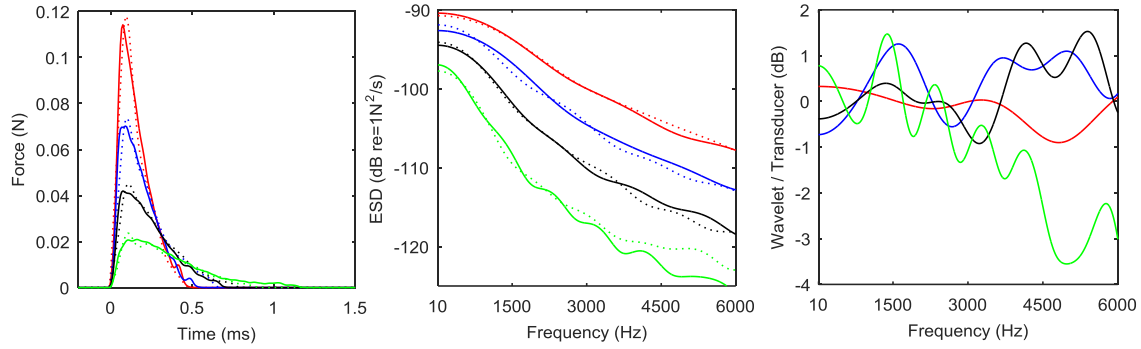

(a) (b) (c)

Figure 6. 2mm drops released from different height impacting on dry glass surface: (a) time-dependent force (b) energy spectrum density (10 - 6k Hz): (H=3.25m: wavelet red line, force transducer red dotted line; H=1.63m: wavelet blue line, force transducer blue dotted line; H=0.81m: wavelet black line, force transducer black dotted line; H=0.41m: wavelet green line, force transducer green dotted line;); (c) difference between wavelet deconvolution and force transducer disc measurement.

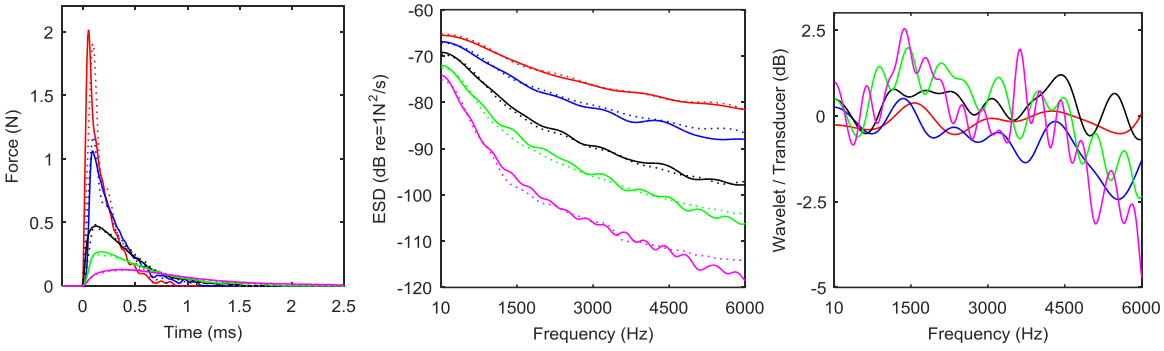

(a) (b) (c)

Figure 7. 4.5mm drops released from different height impacting on dry glass surface: (a) time-dependent force (b) energy spectrum density (10 - 6k Hz): (H=6.5m: wavelet red line, force transducer red dotted line; H=3.25m: wavelet blue line, force transducer blue dotted line; H=1.63m: wavelet black line, force transducer black dotted line; H=0.81m: wavelet green line, force transducer green dotted line; H=0.41m: wavelet magenta line, force transducer magenta dotted line); (c) difference between wavelet deconvolution and force transducer disc measurement.

6. Conclusions

The time-dependent force applied by a single water drop impacting a sheet of glass has been measured with a wavelet deconvolution method and validated against measurements with a glass disc on a force transducer. The wavelet approach has been used to determine an empirical formula to calculate the impact force on dry glass; this gives a more realistic representation of the time-dependence and peak force than predictions assuming an idealized drop shape. The next stage is to use the validated wavelet approach to measure impacts on wet glass.

ACKNOWLEDGEMENT

The authors are very grateful to Dr Gary Seiffert for his help with the experimental set-up.

REFERENCES

1 Nearing, M. A., Bradford J. M., Holtz, R. D., Measurement of force vs. time relations for waterdrop impact, Soil Science Society of America Journal 50(6), 1532-1536, (1986).

2 Nearing, M. A. and Bradford J. M., Relationships between waterdrop properties and forces of impact, Soil Science Society of America Journal 51(2), 425-430, (1987).

3 Grinspan, A. S., and Gnanamoorthy, R., Impact force of low velocity liquid droplets measured using piezoelectric PVDF film, Colloids and Surfaces A: Physicochemical and Engineering Aspects 356(1), 162-168, (2010).

4 Soto, D., De Lariviere, A.B., Boutillon, X., Clanet, C. and Quéré, D., The force of impacting rain, Soft matter 10(27), 4929-4934, (2014).

5 Mitchell, B. R., Nassiri, A., Locke, M. R., Klewicki, J. C., Korkolis, Y. P., & Kinsey, B. L., Experimental and Numerical Framework for Study of Low Velocity Water Droplet Impact Dynamics. In ASME 2016 11th International Manufacturing Science and Engineering Conference. ASME. (2016).

6 Doyle, J. F., A wavelet deconvolution method for impact force identification, Experimental Mechanics 37(4), 403-408, (1997).

7 Petersson, B. A. T., The liquid drop impact as a source of sound and vibration, Building Acoustics 2, 585-624, (1995).

8 Roisman, Ilia V., Romain R., and Cameron T., Normal impact of a liquid drop on a dry surface: model for spreading and receding, Proceedings of the Royal Society of London A: Mathematical, Physical and Engineering Sciences, 458, 1411-1430, (2002).

9 Anantharamaiah, N., Vahedi Tafreshi, H., and Pourdeyhimi, B., A study on hydroentangling waterjets and their impact forces. Experiments in fluids 41(1), 103, (2006).

10 Suga, H., and Tachibana, H., Sound radiation characteristics of lightweight roof constructions excited by rain. Building Acoustics, 1(4), 249-270, (1994).

11 Hopkins, C., Sound insulation. Routledge, 2012. ISBN: 978-0-7506-6526-1.

12 Rein M., Phenomena of liquid drop impact on solid and liquid surfaces. Fluid Dynamics Research, 12(2), 61-93, (1993).

13 Vaseghi, S. V., Advanced signal processing and digital noise reduction. Ch. 5. Springer-Verlag, (2013).

14 Paige, C. C., and Saunders, M. A., LSQR: An algorithm for sparse linear equations and sparse least squares. ACM transactions on mathematical software 8(1), 43-71, (1982).

15 Chang, C., Sun, C. T., Determining transverse impact force on a composite laminate by signal deconvolution. Experimental mechanics, 29(4), 414-419, (1989).

16 Guigon, R., Chaillout, J. J., Jager, T. and Despesse, G., Harvesting raindrop energy: experimental study. Smart Materials and Structures 17(1), 015039, (2008).

17 Clift, R, Grace, J. R., Weber, M. E., Bubbles, drops, and particles. Ch. 7. Academic press, (1978).

18 Szakáll, M., Mitra, S. K., Diehl, K., Borrmann, S., Shapes and oscillations of falling raindrops - A review. Atmospheric research, 97(4), 416-425002E, (2010).

19 Beard, K. V., Bringi, V. N., Thurai, M., A new understanding of raindrop shape. Atmospheric Research 97(4), 396-415, (2010).